

Reinforcement learning for optimal error correction of toric codes

Laia Domingo Colomer, Michalis Skotiniotis, and Ramon Muñoz-Tapia

*Física Teòrica: Informació i Fenòmens Quàntics, Departament de Física,
Universitat Autònoma de Barcelona, 08193 Bellaterra (Barcelona) Spain*

(Dated: July 10, 2022)

We apply deep reinforcement learning techniques to design high threshold decoders for the toric code under uncorrelated noise. By rewarding the agent only if the decoding procedure preserves the logical states of the toric code, and using deep convolutional networks for the training phase of the agent, we observe near-optimal performance for uncorrelated noise around the theoretically optimal threshold of 11%. We observe that, by and large, the agent implements a policy similar to that of minimum weight perfect matchings even though no bias towards any policy is given *a priori*.

I. INTRODUCTION

Computation using quantum mechanical systems holds much promise as the ability of quantum systems to exist in exotic states, such as quantum entanglement and superposition, is known to yield significant advantages in computation [1, 2], communication [3], and sensing [4, 5]. Due to the fragility of such exotic states to environmental decoherence, the ability to actively protect sensitive quantum information against noise by quantum error correction [6, 7] is indispensable on the road to a fully fault-tolerant quantum computing infrastructure [8]. Quantum error correcting codes (QECC) need to be efficiently implementable both in terms of the physical operations as well as the time needed to recover corrupted quantum data. A promising platform are topological error correcting codes (TECC) [9, 10] for which the recovery operations consist of quasi-local error-syndrome measurements and local Pauli correction operations. A drawback of TECC is that the error configuration space grows prohibitively large with the number of errors, and error syndromes exhibit high degeneracy making the design of optimal, fast decoders a highly non-trivial task.

In recent years several approaches based on cellular-automata [11–13], renormalization group [14, 15], restricted Boltzmann machines [16], and machine learning [17–26] have produced a plethora of high performance decoders for both QECC as well as TECC. Particularly for TECC decoders designed using these techniques have shown to achieve similar performance to the best known decoder based on the minimum weight perfect matchings (MWPM) algorithm [27].

Here we construct model-free optimal decoders for the toric code [9] in the presence of uncorrelated noise. We use deep convolutional networks and episodic memory to train an agent in a reinforcement learning paradigm. We adopt a model-free approach by considering a system of rewards based solely on whether the agent has successfully recovered the encoded information. We find significant performance improvement just shy of the optimal threshold. DQL produces decoding strategies with slightly higher threshold than those based on policy-driven reinforcement learning scenarios [26] under similar training conditions. Our approach exhibits

good performance even when trained with error rates slightly above percolation. We find that our model-free decoders indeed implement a policy similar to MWPM.

The article is structured as follows. In Sec. II we briefly review the principles of QECC and the stabiliser formalism and introduce TECC and in particular the toric code. In Sec. III we introduce the interaction-based learning scenario between an agent and an environment and give a basic review of reinforcement learning and its implementation. In Sec. IV we formulate the decoding of the toric code in the presence of uncorrelated noise as a reinforcement learning problem and present the results of applying such decoders of up to 9×9 lattices. We summarize and conclude in Sec. V.

II. QUANTUM ERROR-CORRECTION AND THE TORIC CODE

Quantum information deals with the storage, transmission and manipulation of information represented in the states of quantum mechanical systems. Unfortunately, quantum systems are notoriously sensitive to the effects of noise which implies that their information depletes fairly quickly. A way to counteract the deleterious effects of noise is to make use of quantum error correcting codes (QECC) (see [28] and references therein). Much like classical error correction the idea behind QECC is to use a number, n , of *physical* quantum systems, each with an associated state space \mathcal{H} , and identify a suitable subspace, $\mathcal{C} \subset \mathcal{H}^{\otimes n}$, onto which quantum information can be protected by decoherence. A crucial ingredient in QECC are the encoding and decoding operations to and from the *code space* \mathcal{C} . Ideally we seek to design codes with large error tolerance, high storage capacity, and efficient encoding, decoding and recovery operations. Hereafter, all physical systems we consider are two-dimensional quantum systems (qubits).

The dimension, d , of the code space, \mathcal{C} , defines the number of distinct *logical* states, or codewords, as well as the number of *logical* qubits, $k = \log d$. The *distance*, δ , of a code is the number of errors it can correct. By way of example, the three-qubit repetition code utilizes the code space $\mathcal{C} := \text{span}\{|0\rangle_L \equiv |000\rangle, |1\rangle_L \equiv |111\rangle\}$,

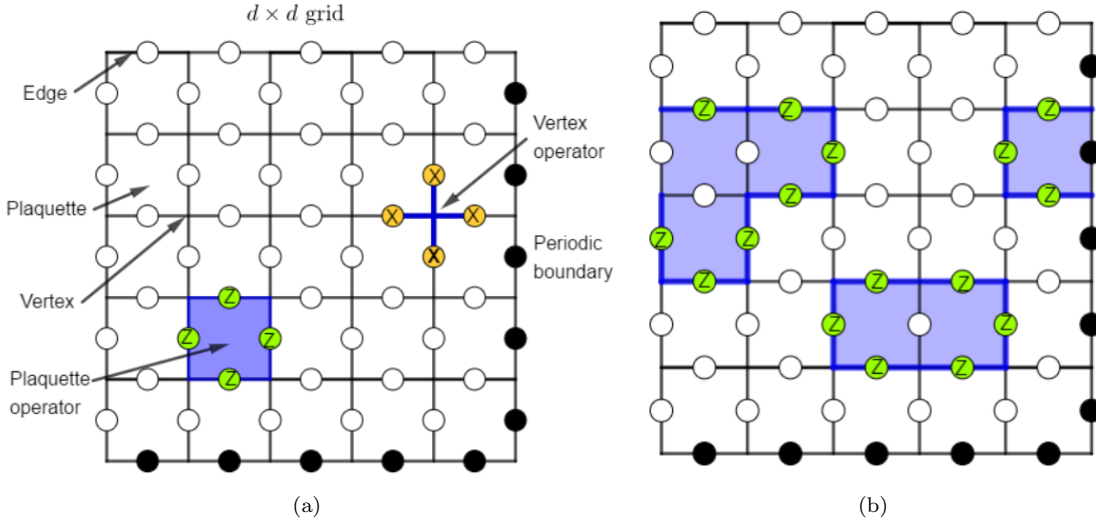


FIG. 1. The basic ingredients of the toric code: (a) A 5×5 lattice with the topology of a torus. The right and left boundaries of the lattice satisfy one periodic boundary condition, whereas the top and bottom edges the other periodic boundary condition. Physical qubits—represented as circles—are placed on the edges of the lattice. The stabilizers of the toric code are associated with *plaquette* operators (shaded blue square), and *vertex* operators (dark blue star) (b) Examples of multiplication of plaquette operators. The resultant operator consists of Z operators acting on the boundary of the combined plaquettes, and correspond to a stabilizer operator.

of three physical qubits to store one logical qubit and protect it against a single qubit X error. Here we denote by

$$X = \begin{pmatrix} 0 & 1 \\ 1 & 0 \end{pmatrix}, \quad Y = \begin{pmatrix} 0 & -i \\ i & 0 \end{pmatrix}, \quad Z = \begin{pmatrix} 1 & 0 \\ 0 & -1 \end{pmatrix}, \quad (1)$$

the usual Pauli matrices.

As the number of physical qubits and error thresholds for QECC grows working directly with logical states and their superpositions becomes inefficient. Thankfully, an efficient description of QECCs exists in terms of the stabilizer formalism [29, 30]. A subspace $\mathcal{C} \subset \mathcal{H}^{\otimes M}$ is said to be *stabilized* by an operator $P \in \mathcal{B}(\mathcal{H}^{\otimes M})$ if for any $|\psi\rangle \in \mathcal{C}$, $P|\psi\rangle = |\psi\rangle$. If this is the case then P is called a *stabilizer* of the code and \mathcal{C} is uniquely specified as the eigenspace of the complete set of commuting stabilizers $\mathcal{P} := \{P_i, i \in (1, \dots, N) | [P_i, P_j] = 0, \forall i \neq j\}$ with eigenvalue $+1$. Note that \mathcal{P} forms a finite Abelian group under matrix multiplication and consequently can be generated by $m = \log(N)$ suitably chosen generators. The number of generators m , logical qubits k , and physical qubits n are related by $m = n - k$.

In order to encode logical quantum information we need to construct the logical Pauli operators, X_L, Z_L in such a way that they commute with the stabiliser group \mathcal{P} . For the three-qubit code, we have

$$\mathcal{P} = \{Z \otimes Z \otimes \mathbf{1}, \quad Z \otimes \mathbf{1} \otimes Z, \quad \mathbf{1} \otimes Z \otimes Z, \quad \mathbf{1} \otimes \mathbf{1} \otimes \mathbf{1}\}, \quad (2)$$

and one can easily check that the following operators

$$X_L = X \otimes X \otimes X \quad Z_L = Z \otimes \mathbf{1} \otimes \mathbf{1}, \quad (3)$$

commute with those of Eq. (2), and satisfy the Pauli commutation relations.

Decoding, on the other hand, is a two-stage process involving first a recovery operation before extracting the relevant quantum information. The recovery operation consists of measuring all 2^m stabilizers and, based on the measurement outcomes—the *error syndrome*—apply Pauli correction operations on the n physical qubits. If the syndrome contains all $+1$ then no recovery operation is required, whereas -1 values in the syndrome indicate the presence of errors. For the three-qubit code, $m = 3 - 1 = 2$. The error syndromes of $Z \otimes Z \otimes \mathbf{1}$ and $\mathbf{1} \otimes Z \otimes Z$ uniquely identify the physical qubit on which a Pauli X error occurred. Note, however, that in general the relationship between physical errors and the syndrome read-out is not unique. There may be many error configurations which lead to the same syndrome, a phenomenon that occurs frequently in topological QECC which we now review.

Topological QECC: the toric code

Constructing QECC with high capacity for quantum information and large distance poses a serious challenge as both stabilizers and logical operations are generally *global* operators acting on all n physical qubits. An alternative, and more resource intensive, way of constructing QECCs is to exploit the topological properties of multi-qubit systems arranged on a lattice [9, 10]. Such topological error correcting codes attain superb protection from decoherence, while requiring only local gates for error-correction and have been experimentally constructed in a variety of architectures [31–37]. In the remainder of this work, we shall focus on one of the

simplest TECC, the toric code [9].

The toric code defined over an $d \times d$ square lattice, consists of $n = 2d^2$ physical qubits placed on every edge of the lattice. The topology of the torus arises from two distinct boundary conditions, one for the left and right edge of the lattice and one for the top and bottom edges. The stabilizer group of the toric code is generated by two distinct stabilizers associated with the plaquettes and vertices of the lattice [see Fig. 1(a)]. Specifically, to every plaquette, p , and vertex v , the operators

$$P_p = \bigotimes_{j \in \text{boundary}(p)} Z_j, \quad Q_v = \bigotimes_{j \in \text{vertex}(v)} X_j \quad (4)$$

are stabilizers of the toric code, and there are a total of $2(d^2 - 1)$ independent plaquette and vertex operators forming the generators of its stabilizer group. Observe that adjacent plaquette and vertex operators commute as they overlap on exactly two physical qubits. Products of plaquette (vertex) operators are also stabilizers of the torus and give rise to *trivial loops* as illustrated in Fig. 1(b).

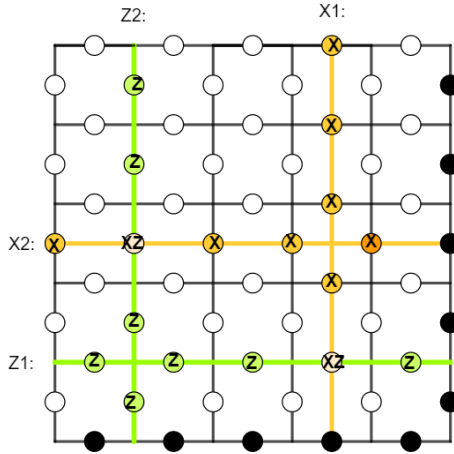


FIG. 2. The logical Pauli operators $\{X_L^{(i)}, Z_L^{(i)}\}_{i=1}^2$.

The dimension of the code space is $2d^2 - 2(d^2 - 1) = 2$. The logical operators, $\{X_L^{(i)}, Z_L^{(i)}\}_{i=1}^2$, for each of the logical qubits are shown in Fig. 2. They form *non-trivial* closed loops around the torus with $Z_L^{(1)}$ forming horizontal loops, $Z_L^{(2)}$ vertical loops and the corresponding $X_L^{(i)}$ being closed loops orthogonal to those of $Z_L^{(i)}$. Notice, however, that the construction of the logical operators is not unique: we can generate an equivalence class of logical operators, acting identically on the code space, by multiplying the above logical operators with elements of \mathcal{P} (i.e., the loops do not need to be straight).

From the preceding discussion it follows that for a logical error to occur, an odd number of non-trivial loops around the torus must occur. Therefore, the distance of the toric code is d . If a physical qubit suffers an error, the stabilizer generators adjacent to the position of the physical qubit will have error syndrome -1 . Left

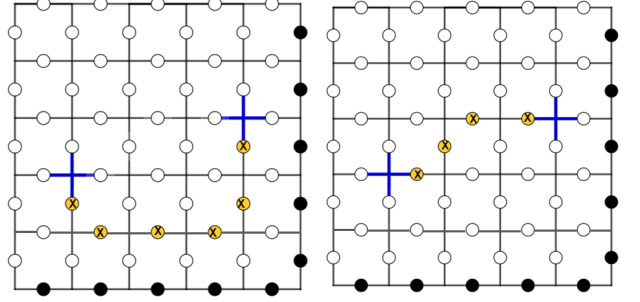


FIG. 3. Example of different physical errors (orange circles) leading to the same vertex syndrome error (blue lines crossing a vertex).

unaddressed, the accumulation of errors may result in non-trivial loops around the torus and thus to logical errors. So we must actively perform recovery operations, but we must be extremely careful on how to do these, as several configurations of physical errors correspond to the same error syndrome as shown in Fig. 3. In addition, the design of optimal decoders also relies heavily on the types of errors occurring as well as their distribution. The simplest and most common noise models assume that each qubit experiences an independent and identically distributed (i.i.d.) noise process, with a probability p of suffering an error. Among the uncorrelated noise models, the most relevant ones are bit-flip (X errors) and phase-flip (Z errors) errors. For *correlated* errors depolarizing noise (X, Y, Z noise each with probability $p/3$) is the most paradigmatic noise model. In this work we shall only consider uncorrelated noise and without loss of generality we shall assume bit-flip noise (analysis for phase-flip errors is completely parallel). Correlated noise is more challenging and will be addressed in future work. The optimal threshold of a decoder, on the other hand, is the maximum value of p for which recovery of the information is possible. For the toric code under i.i.d bit-flip errors this threshold is known to be 11% [38].

A widely used decoder for the toric code under bit-flip errors is based on the MWPM algorithm [39, 40]. MWPM adopts the policy of correcting for the most likely error given a particular error syndrome and has proven to be a very successful decoder with an estimated threshold of 10.3% [41]. Recently, machine learning techniques and applications of (deep) neural networks have been applied in search for optimal decoders, both for topological as well as standard QECC [17–26]. We now review the main techniques in reinforcement learning which we will use in search of efficient decoders for the toric code.

III. REINFORCEMENT LEARNING

Reinforcement learning (RL) is a framework within which one can precisely formulate the old dictum of “learning through experience” [42]. Agents trained using RL have excelled at performing certain tasks, such as mastering the game of Go [43], better than humans and RL based agents are used extensively in robotics [44], artificial intelligence [45], and face-recognition [46]. Here we introduce the agent-environment paradigm of RL and review its key features; state and action valued functions. We then briefly discuss deep Q-learning (DQL) which uses deep convolutional networks highlighting some key techniques used to guarantee convergence in the training process for the agent.

Consider a scenario involving an agent, A , sequentially interacting with its immediate environment, E , in order to learn how to achieve a specific task (see Fig. 4). Here, learning is to be understood as A ’s ability to refine its future behaviour based on past experience in order to maximise future reward. Regardless of the details of A , E , and their interaction any such learning scenario can be modelled using the following three ingredients [42]: the set of all possible states, \mathcal{S} , of E , the set of all possible actions, \mathcal{A} , of A , and the set of rewards, \mathcal{R} —an assessment of A ’s performance towards the task. If the interaction is known, then one talks of *model-based* RL, otherwise the latter is *model-free*.

The learning process of A can be described in terms of episodes [47]. A and E interact, as shown in Fig. 4, and the episode finishes when the agent reaches the terminal state. Any given step $k \in \mathbb{Z}_N$ in an episode consists of A receiving the reward $r_k \in \mathcal{R}_k \subseteq \mathcal{R}$ —from her/his previous action—and the current state of E , $s_k \in \mathcal{S}_k \subseteq \mathcal{S}$. A then performs action $a_k \in \mathcal{A}_k \subseteq \mathcal{A}$, after which E sends reward $r_{k+1} \in \mathcal{R}_{k+1}$, and its state changes to $s_{k+1} \equiv \mathcal{E}(s_k) \in \mathcal{S}_{k+1} \subseteq \mathcal{S}$.

The set of states, rewards, and actions of an episode are random variables, and the interaction between A and E is a stochastic map $\mathcal{E}_k : \mathcal{S}_k \rightarrow \mathcal{S}_{k+1}$, that may depend on all preceding states of E and actions of A . Specifically, the probability that A receives reward r_{k+1} , and the state of E at step $k+1$ is s_{k+1} , given all preceding states $s_k = s_1 s_2 \dots s_k$ and actions $a_k = a_1 a_2 \dots a_k$ is $p(s_{k+1}, r_{k+1} | s_k, a_k)$. If the conditional probabilities depend solely on the last preceding state of E and action of A , i.e., $p(s_{k+1}, r_{k+1} | s_k, a_k) = p(s_{k+1}, r_{k+1} | s_k, a_k), \forall s_{k+1}, s_k, r_{k+1}$, and a_k then every finite sequence of steps is formally equivalent to a finite Markov decision process (MDP) [48]. The average reward an agent A expects to obtain after performing action a_k , given the state of the environment is s_k , is then

$$\mathbb{E}[r_{k+1}(s_k, a_k)] = \sum_{r_{k+1} \in \mathcal{R}_{k+1}} r_{k+1} \sum_{s_{k+1} \in \mathcal{S}_{k+1}} p(s_{k+1}, r_{k+1} | s_k, a_k). \quad (5)$$

Note that whilst we have assumed that both state and

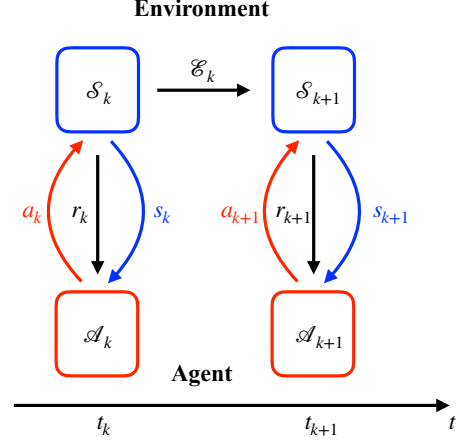


FIG. 4. A step in an episode in a general RL problem. The agent receives reward r_k from her/his previous action while the current state of the environment is $s_k \in \mathcal{S}_k$. The agent performs action $a_k \in \mathcal{A}_k$ which causes the environment to update its state to $s_{k+1} = \mathcal{E}_k(s_k)$, and reward the agent with $r_{k+1} \in \mathcal{R}_{k+1}$. This interaction is repeated until a terminal state s_T is reached, and the episode finishes. The sequence $\{(r_k, s_k, a_k)\}_{k=1}^T$ within the episode is called *trajectory*.

action spaces are finite dimensional, Eq. (5) can be equally applied to infinite dimensional cases.

The learning of the agent is quantified by the *expected discounted return*

$$R_k := \sum_{n=0}^T \gamma^n r_{k+n+1}, \quad (6)$$

where $0 \leq \gamma \leq 1$ is the *discount rate* [49]; $\gamma = 0$ favours immediate rewards, whereas for $\gamma = 1$ future rewards are favoured. The decision making process of A is known as a *policy* and consists of a complete specification of the actions A will perform at every step of the sequence and for any possible state of E . Given a state s_k the probability that A will perform action a_k is denoted by $\pi(a_k | s_k)$. Under a policy π the value of a state s_k , $v_\pi(s_k)$, quantifies its average expected future returns, i.e., $v_\pi(s_k) = \mathbb{E}[R_k | s_k]_{\pi(\mathcal{A}_k | s_k)}$. Similarly, the value of an action a_k given a state s_k —known as the *q-value* $q_\pi(s_k, a_k)$ —quantifies the average expected future returns of that action, i.e., $q_\pi(s_k, a_k) = \mathbb{E}[R_k | s_k, a_k]_{\pi(\mathcal{A}_{k+1}, a_k | s_{k+1}, a_k)}$. Such policy-valued functions induce a partial order in the space of all possible policies of an agent: π is at least as good as π' , if and only if $v_\pi(s_k) \geq v_{\pi'}(s_k), \forall s_k \in \mathcal{S}_k$. A policy π^* is optimal if no other policy can give a higher value than it, $v_{\pi^*}(s_k) = \max_\pi v_\pi(s_k)$ [42].

To determine the optimal policy one makes use of the recursive nature of both $v_\pi(s_k)$, and $q_\pi(s_k, a_k)$ to write

$$v_\pi(s_k) = \sum_{a_k \in \mathcal{A}_k} \pi(a_k | s_k) \sum_{s_{k+1}} \sum_{r_{k+1}} p(s_{k+1}, r_{k+1} | s_k, a_k) \times (r_{k+1} + \gamma v_\pi(s_{k+1})), \quad (7)$$

and

$$q_\pi(s_k, a_k) = r_{k+1}(s_k, a_k) + \gamma q_\pi(s_{k+1}, a_{k+1}). \quad (8)$$

Eqs. (7), and (8) are known as the *Bellman* equations [50] for state and action-valued functions. For the optimal policy π^* , $v_{\pi^*}(s_k)$ takes the specific form

$$v_{\pi^*}(s_k) = \max_{a_k \in \mathcal{A}_k} \sum_{s_{k+1}} \sum_{r_{k+1}} p(s_{k+1}, r_{k+1} | s_k, a_k) \times (r_{k+1} + \gamma v_{\pi^*}(s_{k+1})) \quad (9)$$

known as the Bellman optimality equation. Note that an optimal policy is known to always exist, though it may not be unique [51].

Agent training: Deep Q-learning

If the environment in a MDP is known then the optimal policy can be obtained by solving $|\mathcal{S}|$ Bellman equations. For model-free RL no such possibility exists and consequently state and action valued functions need to be estimated from experience. A typical algorithm used in this case is called *Q-learning*, with guaranteed convergence to the optimal *q*-value if every state-action pair is observed sufficiently large number of times, i.e., if the agent is trained infinitely long [42]. For large state spaces this is prohibitively expensive. Consequently we have to resort to finite training sets which in turn means that the agent will often encounter situations previously unseen.

Deep Q-learning (DQL) uses deep convolutional networks [52], specialised for processing high-dimensional data, in order to extract global features and patterns. Upon encountering a previously unseen state, DQL uses such global features to compare with similar situations in past experience [53]. DQL parametrises the *q*-function in terms of a neural network, so that given an input state and action, the neural network produces the *q*-value $q(s, a)$ as an output. During training, the network parameters are adjusted, via stochastic gradient descent, such as to reduce the error between the optimal and approximated target *q*-values.

We use DQL to train our agent to successfully decode uncorrelated bit or phase flip noise on the toric code. Training halts either after a certain number of episodes have happened, or until the loss function of the convolutional neural network stops decreasing. To ensure stability during training we also make use of additional training techniques, such as double deep Q-learning, dueling deep Q-learning, and prioritised experience replay [54, 55].

IV. DEEP RL DECODERS FOR UNCORRELATED NOISE

We now cast decoders for the toric code under uncorrelated noise as a RL problem and present the results of

training model-free agents to accomplish the task. As already mentioned we discuss only the case of bit-flip errors. The environment, E , consists of the state of the toric code; a matrix of $2d^2$ entries containing the position of errors applied to the physical qubits for any given episode. This state is hidden from A and it is used to generate the state space \mathcal{S}_k , by providing the error syndrome of all stabilisers \mathcal{P} of the code, in this case a set of $d \times d$ matrices representing the position of each stabilizer and its corresponding error syndrome.

The agents actions consist of single qubit bit flip operations. In principle, we can allow the agent to act on any of the $2d^2$ qubits. However, training can be significantly sped-up by feeding the algorithm with a convenient representation of the errors. Because of the boundary conditions of the torus, the syndrome error of any stabilizer can be represented as an arbitrary plaque at the center of the torus [26]. For each syndrome we can generate a set of matrices—the *perspectives* B_i —each of them having a different defect at its center while keeping the relative position of other defects fixed. The input to the neural network are the perspectives B_i , for which the neural network provides the *q*-value for each of the four possible actions; X corrections on the qubits adjacent to the vertex in question. A applies the action with the highest *q*-value. This way for a syndrome error involving N errors, the agent has to choose among $4N$ possible actions.

The agent continues to perform actions until the *terminal state* of the environment is reached: all syndrome measurements have outcome +1. As we compute the actions A performs on the hidden state of the code along the way we can evaluate the number of non-trivial horizontal or vertical loops around the torus. If an even number of such loops is found, no logical errors have occurred and the agent is rewarded a nominal reward of $r = +1000$ [56]. Else, the agent's reward is $r = 0$. In [26], a RL decoder for the same decoder was designed using similar techniques as ours. There the agent was penalised with $r = -1$ for every iteration, so that the optimal strategy would be to correct the error syndrome with the minimum number of operations. This strategy is based on adopting a particular policy, namely that of the MWPM algorithm. We compare this reward scheme with ours.

We train the agent using the DQL algorithm, until the parameters of the convolutional neural network stabilize. In order to give the agent more freedom to explore the large policy space during training we use an ϵ -greedy strategy for *Q*-learning; with probability $1 - \epsilon$ the agent selects the action with the highest value of the current *q*-function, whereas with probability ϵ the agent performs an action at random. Furthermore, we vary the value of ϵ during training, linearly decreasing it to the minimum value of $\epsilon = 0.1$. Moreover, we also train the agent with an initially low probability of bit flip errors so that A learns to correct properly, linearly increasing the occurrence of errors near-to and beyond the 11% threshold of the code.

Results

We now present our results on RL decoders for uncorrelated noise on the toric code. Agents were trained on grids of dimensions, $d = 3, 5, 7$ and 9 . After training, we evaluated the decoders performance for different error probabilities p . We define the logical success probability as the proportion of syndromes decoded successfully. As for uncorrelated errors the MWPM algorithm is near-optimal, we also compare the RL agent's performance with the MWPM performance of [26].

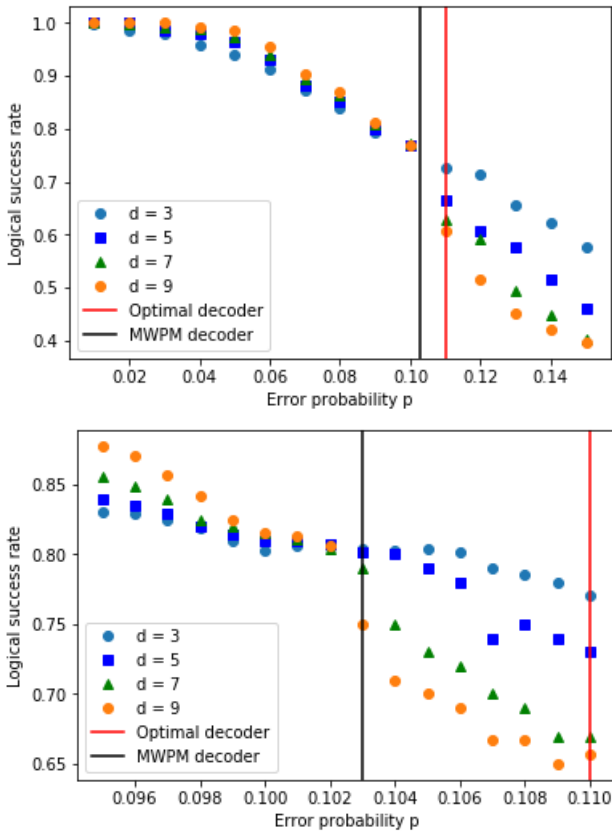


FIG. 5. Logical success probability as a function of error probability p for agents trained in different lattice dimensions $d = 3, 5, 7, 9$. The values of p range from $0.01 - 0.15$ (top) and from $0.095 - 0.11$ (bottom). All agents were trained with error probability $p = 0.10$. Thresholds for the optimal decoder and the MWPM decoder are shown as red and grey vertical bars, respectively.

Fig. 5 shows the logical success probability as a function of the error probability p for several lattice sizes between the RL decoder based on MWPM and our model-free decoder. For $p \leq 0.10$ the performance of the RL agent improves with the dimension d of the lattice. When the error probability p is low, the probability of successful decoding increases with the dimension of the lattice, whereas for p high the opposite effect occurs. The turning point between these two behaviours is called the *code threshold*. The code threshold for

these agents falls between $p = 0.102$ and $p = 0.103$, slightly higher than those based on MWPM. We also tested decoders which were trained with error probabilities higher than the code threshold $p = 0.15$, and $p = 0.2$. We noticed a slight increase in performance in the former case whilst in the latter decoders performed significantly worse.

A more direct comparison between our decoder and the one based on MWPM is shown in Fig. 6. We trained an agent according to the reward system of [26], which implements the MWPM algorithm, and compared the episode length distribution for both agents. For $d = 5$

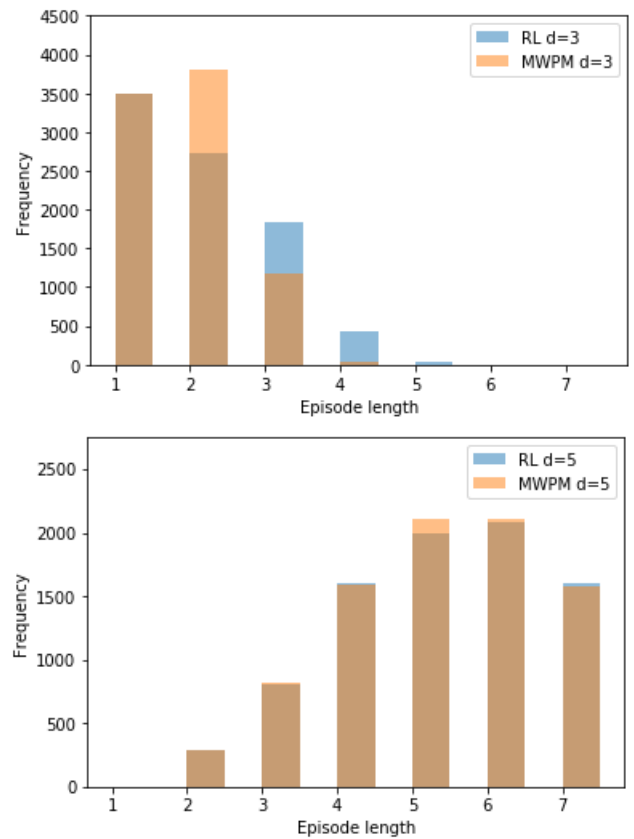


FIG. 6. Episode length distribution for agents trained to simulate the MWPM algorithm and agents trained based on rewarding solely on successful decoding for $d = 3$ (top) and $d = 5$ (bottom).

both agents seem to have very similar episode length distributions meaning that an agent trained based on success/failure reward learnt that, in general, the best strategy is indeed MWPM even though it was not explicitly told so. For $d = 3$, the episode length distributions are more distinct. By and large the agent adopts a decoding strategy requiring the least amount of corrections but occasionally slightly more steps are required.

Our results indicate that it is not necessary to train agents to follow the MWPM policy, our model-free decoder is able to learn the best policy and yield even better recovery rates. A comparison of the efficiencies

of the two decoders is shown in Fig. 7. For $d = 5$ both

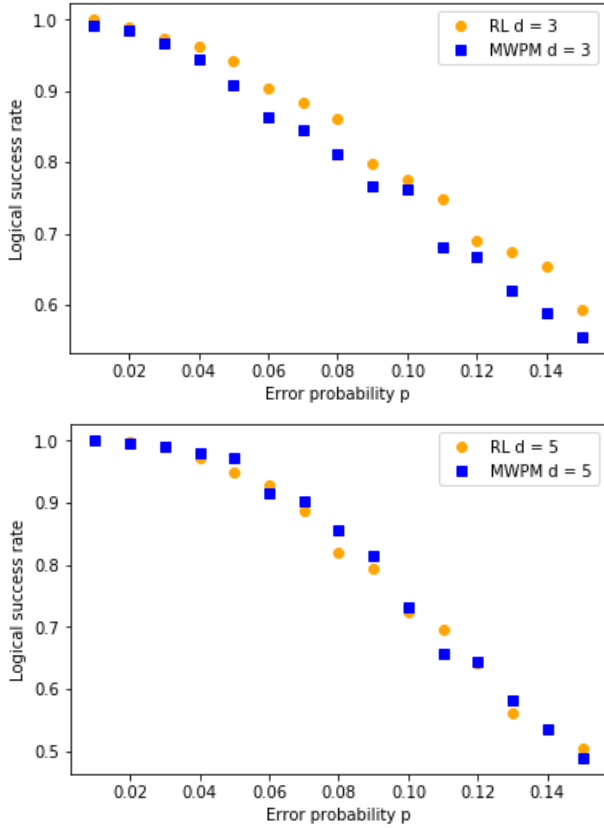


FIG. 7. Logical success probability as a function of error probability p for agents trained with success/failure rewards and MWPM rewards for $d = 3$ (top) and $d = 5$ (bottom).

agents have very similar success probability. However, for $d = 3$, the agent trained with success/failure rewards

outperforms the MWPM agent indicating that the different policy adopted by the success/failure agent is in fact beneficial for correct decoding of the code.

V. SUMMARY AND CONCLUSIONS

In this work we used deep Q-learning to train an agent using reinforcement learning in order to decode uncorrelated errors on a toric code. We showed that rewarding the agent only if the decoding procedure yields no logical errors, leads to slightly better performance as compared to more policy-orientated rewards, and achieves near-optimal performance. Moreover, by comparing the episode length distributions of our decoding scheme with those of an agent implementing MWPM we observed that indeed policies based on the latter seem to form the most efficient decoders.

Unlike policy-driven algorithms we believe that our model-free scheme of choosing rewards based solely on the success/failure of the decoding procedure is more versatile and can be used to design decoders for other TECC, , such as surface codes, or the Kagome lattice, as well as for more general noise models. We expect that our approach is able to address error correction for correlated noise for which policy-driven methods are unsuitable. Work along this line is currently under consideration.

ACKNOWLEDGEMENTS

The authors acknowledge support from Spanish MINECO reference FIS2016-80681-P (with the support of AEI/FEDER,EU); the Generalitat de Catalunya, project CIRIT 2017-SGR-1127 and the Baidu-UAB collaborative project ‘Learning of Quantum Hidden Markov Models’.

[1] A. Galindo and M. A. Martín-Delgado, *Rev. Mod. Phys.* **74**, 347 (2002).

[2] I. M. Georgescu, S. Ashhab, and F. Nori, *Rev. Mod. Phys.* **86**, 153 (2014).

[3] N. Gisin and R. Thew, *Nat. Photonics* **1**, 165 (2007).

[4] V. Giovannetti, S. Lloyd, and L. Maccone, *Nat. Photonics* **5**, 222 (2011).

[5] C. L. Degen, F. Reinhard, and P. Cappellaro, *Rev. Mod. Phys.* **89**, 035002 (2017).

[6] D. Gottesman, in *Quantum information science and its contributions to mathematics, Proceedings of Symposia in Applied Mathematics*, Vol. 68 (2010) pp. 13–58.

[7] B. M. Terhal, *Rev. Mod. Phys.* **87**, 307 (2015).

[8] E. T. Campbell, B. M. Terhal, and C. Vuillot, *Nature* **549**, 172 (2017).

[9] S. B. Bravyi and A. Kitaev, arXiv preprint quant-ph: 9811052 (1998).

[10] H. Bombín, arXiv preprint quant-ph: 1311.0277 (2013).

[11] M. Herold, E. T. Campbell, J. Eisert, and M. J. Kastoryano, *npj Quantum information* **1**, 15010 (2015).

[12] M. Herold, M. J. Kastoryano, E. T. Campbell, and J. Eisert, *New J. Phys.* **19**, 063012 (2017).

[13] N. Lang and H. P. Büchler, *SciPost Phys.* **4**, 007 (2018).

[14] G. Duclos-Cianci and D. Poulin, in *2010 IEEE Information Theory Workshop* (IEEE, 2010) pp. 1–5.

[15] G. Duclos-Cianci and D. Poulin, *Phys. Rev. Lett.* **104**, 050504 (2010).

[16] G. Torlai and R. G. Melko, *Phys. Rev. Lett.* **119**, 030501 (2017).

[17] S. Varsamopoulos, B. Criger, and K. Bertels, *Quantum Science and Technology* **3**, 015004 (2017).

[18] S. Krastanov and L. Jiang, *Sci Rep-UK* **7**, 11003 (2017).

[19] P. Baireuther, T. E. O’Brien, B. Tarasinski, and C. W. Beenakker, *Quantum* **2**, 48 (2018).

[20] T. Fösel, P. Tighineanu, T. Weiss, and F. Marquardt, *Phys. Rev. X* **8**, 031084 (2018).

- [21] C. Chamberland and P. Ronagh, *Quantum Science and Technology* **3**, 044002 (2018).
- [22] R. Sweke, M. S. Kesselring, E. P. van Nieuwenburg, and J. Eisert, arXiv preprint arXiv:1810.07207 (2018).
- [23] H. P. Nautrup, N. Delfosse, V. Dunjko, H. J. Briegel, and N. Friis, arXiv preprint quant-ph: 1812.08451 (2018).
- [24] Y.-H. Liu and D. Poulin, *Phys. Rev. Lett.* **122**, 200501 (2019).
- [25] S. Varsamopoulos, K. Bertels, and C. G. Almudever, arXiv preprint arXiv:1901.10847 (2019).
- [26] P. Andreasson, J. Johansson, S. Liljestrand, and M. Granath, *Quantum* **3**, 183 (2019).
- [27] J. Edmonds, *Can. J. Math.* **17**, 449467 (1965).
- [28] D. A. Lidar and T. A. Brun, *Quantum error correction* (Cambridge university press, 2013).
- [29] D. Gottesman, *Stabilizer Codes and Quantum Error Correction*, Ph.D. thesis, California Institute of Technology (1997).
- [30] D. Poulin, *Phys. Rev. Lett.* **95**, 230504 (2005).
- [31] X.-C. Yao, T.-X. Wang, H.-Z. Chen, W.-B. Gao, A. G. Fowler, R. Raussendorf, Z.-B. Chen, N.-L. Liu, C.-Y. Lu, Y.-J. Deng, *et al.*, *Nature* **482**, 489 (2012).
- [32] D. Nigg, M. Mueller, E. A. Martinez, P. Schindler, M. Hennrich, T. Monz, M. A. Martin-Delgado, and R. Blatt, *Science* **345**, 302 (2014).
- [33] C. D. Hill, E. Peretz, S. J. Hile, M. G. House, M. Fuechsel, S. Rogge, M. Y. Simmons, and L. C. Hollenberg, *Science Advances* **1**, e1500707 (2015).
- [34] A. D. Córcoles, E. Magesan, S. J. Srinivasan, A. W. Cross, M. Steffen, J. M. Gambetta, and J. M. Chow, *Nat. Commun.* **6**, 6979 (2015).
- [35] J. Kelly, R. Barends, A. G. Fowler, A. Megrant, E. Jeffrey, T. C. White, D. Sank, J. Y. Mutus, B. Campbell, Y. Chen, *et al.*, *Nature* **519**, 66 (2015).
- [36] D. Riste, S. Poletto, M.-Z. Huang, A. Bruno, V. Vesterinen, O.-P. Saira, and L. DiCarlo, *Nat. Commun.* **6**, 6983 (2015).
- [37] M. Takita, A. D. Córcoles, E. Magesan, B. Abdo, M. Brink, A. Cross, J. M. Chow, and J. M. Gambetta, *Phys. Rev. Lett.* **117**, 210505 (2016).
- [38] E. Dennis, A. Kitaev, A. Landahl, and J. Preskill, *J. Math. Phys.* **43**, 4452 (2002).
- [39] H. N. Gabow, *JACM* **23**, 221 (1976).
- [40] W. Cook and A. Rohe, *INFORMS J. Comput.* **11**, 138 (1999).
- [41] D. Browne, “Lectures on topological codes and quantum computation,” (2014), (Accessed on 30/10/2019).
- [42] R. S. Sutton, A. G. Barto, *et al.*, *Introduction to reinforcement learning*, Vol. 2 (MIT press Cambridge, 1998).
- [43] D. Silver, A. Huang, C. J. Maddison, A. Guez, L. Sifre, G. Van Den Driessche, J. Schrittwieser, I. Antonoglou, V. Panneershelvam, M. Lanctot, *et al.*, *Nature* **529**, 484 (2016).
- [44] G. B. Orr and K.-R. Müller, *Neural networks: tricks of the trade* (Springer, 2003).
- [45] S. Ramos, S. Gehrig, P. Pinggera, U. Franke, and C. Rother, in *2017 IEEE Intelligent Vehicles Symposium (IV)* (IEEE, 2017) pp. 1025–1032.
- [46] R. Brunelli and T. Poggio, *IEEE transactions on pattern analysis and machine intelligence* **15**, 1042 (1993).
- [47] Note that we can always consider finite sequences by introducing a terminal state for the environment indicating that the task is completed.
- [48] R. Bellman, *Indiana Univ. Math. J.* **6**, 679 (1957).
- [49] The use of a discount rate is particularly useful for dealing with continuous interactions between agent and environment, i.e., for continuous sequences.
- [50] R. Bellman, *Science* **153**, 34 (1966).
- [51] M. L. Puterman, *Markov decision processes: discrete stochastic dynamic programming* (John Wiley & Sons, 2014).
- [52] N. Kalchbrenner, E. Grefenstette, and P. Blunsom, arXiv preprint arXiv:1404.2188 (2014).
- [53] V. Mnih, K. Kavukcuoglu, D. Silver, A. A. Rusu, J. Veness, M. G. Bellemare, A. Graves, M. Riedmiller, A. K. Fidjeland, G. Ostrovski, *et al.*, *Nature* **518**, 529 (2015).
- [54] V. Mnih, K. Kavukcuoglu, D. Silver, A. Graves, I. Antonoglou, D. Wierstra, and M. Riedmiller, arXiv preprint arXiv:1312.5602 (2013).
- [55] T. Simonini, “Improvements in Deep Q Learning: Dueling Double DQN, Prioritized Experience Replay, and fixed Q-targets,” (2018).
- [56] The value of the reward is chosen so as to speed-up the training process.